

Loop Heat Pipe Wick Fabrication via Additive Manufacturing

Bradley Richard¹, Devin Pellicone², and Bill Anderson³
Advanced Cooling Technologies, Inc., Lancaster, PA, 17601

As the capabilities of CubeSats and SmallSats increase so do the heat rejection requirements. While loop heat pipes (LHPs) are capable of transporting heat across deployable radiators they are currently too expensive for most applications. The largest cost comes from the fabrication of the primary wick which requires multiple machining steps as well as a knife-edge seal. In this work the feasibility of fabricating a loop heat pipe (LHP) primary wick using a direct metal laser sintering (DMLS) process was investigated. 3D printing a LHP wick offers several advantages. The overall cost can be significantly reduced by eliminating multiple machining steps and the risk of failure can be reduced by eliminating the knife-edge seal. The challenge with 3D printing of a LHP primary wick is that a very small pore radius is required to supply sufficient capillary pumping power. Most primary wicks have a pore radius of 1-2 μm . A pore radius and permeability study was conducted using a range of DMLS methods and parameters to optimize for LHP primary wicks. The results of this study was a minimum pore radius of 6 μm which provides a capillary pumping power of 11kPa. A 3D printed primary wick was designed and fabricated with a fully dense outer shell for direct welding to the compensation chamber and vapor line thereby eliminating the knife edge seal. The pore size of this wick was 44 μm which was larger than expected from the pore radius and permeability study. A complete LHP prototype was built and tested to demonstrate the performance of the 3D printed wick.

Nomenclature

A	= cross sectional area	θ	= contact angle
L	= flow length	K	= permeability
P_b	= bubble point pressure	μ	= viscosity
ΔP	= pressure drop	σ	= surface tension
\underline{Q}	= volumetric flow rate		
R_p	= pore radius		

I. Introduction

NASA's CubeSat and SmallSat programs provide the ability to rapidly develop and launch small scale satellite platforms for science research and technology demonstration uses, while reducing costs and increasing efficiency. Conventional spacecraft thermal control systems utilize constant conductance heat pipes (CCHPs) and encapsulated pyrolytic graphite for the passive transport of waste heat. However, pyrolytic graphite is very expensive, and CCHPs are difficult to test on the ground and are not generally used for deployable radiators. Loop heat pipes (LHPs) are another commonly utilized thermal control system for spacecraft, but the manufacturing costs are currently too high to make them viable for most CubeSat/SmallSat applications. In this work a low-cost LHP evaporator was fabricated using a technique called Direct Metal Laser Sintering (DMLS), otherwise known as 3-D printing.

DMLS is a process by which metal structures are made in a layer-by-layer sintering process that selectively melts powdered metal. Geometries should complement the building process which favors upward slanting surfaces and large radii just under horizontal structures. Utilizing the DMLS process, metal parts of the most complex

¹ R&D Engineer, Custom Products Group, 1046 New Holland Ave. Lancaster, PA 17601.

² Lead Engineer, Custom Products Group, 1046 New Holland Ave. Lancaster, PA 17601.

³ Chief Engineer, 1046 New Holland Ave. Lancaster, PA 17601.

geometries are built layer-by-layer directly from 3D CAD models. Unique geometric freedom of design enables DMLS to form cavities and undercuts, which with conventional machining methods can only be produced with great difficulty, if at all. The metal powder is most often melted entirely to create a fully dense, homogenous structure. In the case of a LHP primary wick a porous part must be printed with a pore radius on the order of 1-10 μm in order to have a high enough capillary pressure to overcome the total pressure drop of LHP. A porous part can be accomplished by adjusting the DMLS parameters so that complete melting does not occur, but pore sizes have been limited to >50 μm . In this work a small scale parameter study optimized DMLS parameters to produce porous wicks with pore radii <10 μm .

II. Background

A. Loop Heat Pipe Operation

LHPs are high thermal conductance devices that are self-contained and passive. Figure 1 shows a schematic of a LHP. Note that the figure is not to scale; the vapor and liquid lines can be made much longer. Heat enters the evaporator and vaporizes the working fluid at the interface between the wick and envelope. The vapor is collected by a system of grooves and headers. The vapor flows down the vapor line to the condenser where it condenses as heat is removed by the cold plate. Most of the condenser is filled with a two-phase mixture. A small section at the end of the condenser provides a small amount of liquid sub-cooling.

The compensation chamber (or reservoir) at the end of the evaporator is designed to operate at a lower temperature than the evaporator. The temperature of the compensation chamber can be used to control the operating temperature of the LHP. Since the temperature is lower, the pressure of the saturated fluid in the compensation chamber is also lower. This lower pressure draws the condensate through the condenser and the liquid return line². The fluid then flows into a central pipe where it feeds the wick. Excess fluid drains into the compensation chamber. A secondary wick in the evaporator and compensation chamber allows the liquid in the compensation chamber to feed the evaporator wick. This communication between the compensation chamber and primary wick is required during transient operations. The liquid in the compensation chamber and the interior of the wick must be returned to the exterior surface of the wick to close the cycle. Capillary forces accomplish this passively, pulling liquid back to the surface, similar to water being absorbed into a sponge. Loop heat pipes are made self-priming by carefully controlling the volumes of the compensation chamber, condenser, vapor line and liquid line so that liquid is always available to the wick. The compensation chamber and fluid charge are set so that there is always fluid in the compensation chamber even if the condenser, vapor line and liquid line are completely filled. The LHP is thus inherently self-priming.

B. Loop Heat Pipe Fabrication

The key component of the Loop Heat Pipe system is the pump assembly and its corresponding subcomponents¹. A detailed view of this assembly is shown in Figure 2. The key subcomponents of the pump assembly consist of the cylindrical envelope, a primary wick, a secondary wick, the bayonet, two bi-metallic transition couplings, and the Knife Edge Seal (KES). The compensation chamber is welded to this pump subassembly via one of the bimetallic transitions. The KES is critical for developing the differential pressure required to drive the working fluid around the system. The material selection and installation mechanics for these components are critical to the device's operation for a number of reasons; high sensitivity to heat leak, KES effectiveness, and sensitivity to the thermal resistance through the evaporator body. The material selection required to satisfy these objectives is a large source of the shortcomings associated with its production.

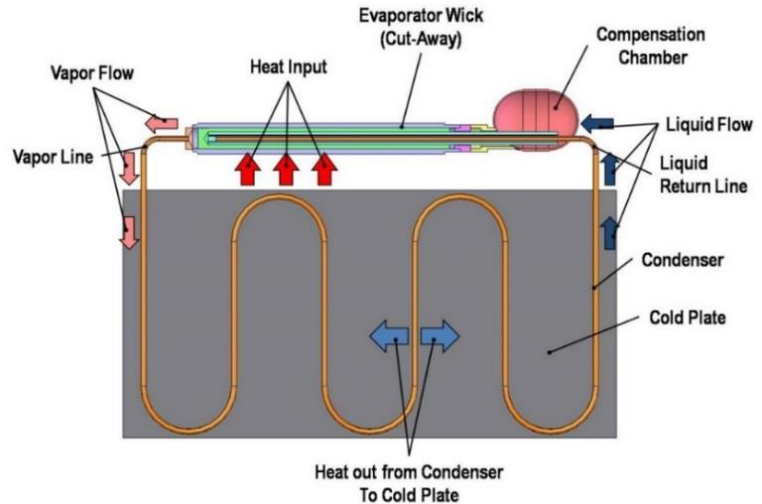


Figure 1. Loop heat pipe schematic (not to scale). For example, the vapor and liquid return lines can be much longer.

Currently, the primary wick structure is produced external from the envelope, using sintered Nickel powder. The fabrication process entails compacting Nickel powder into a sintering mandrel and firing at high temperatures. The oversized wick is then machined at low speeds, and without lubricant to produce the vapor grooves and reduce the outer diameter to the proper size while preventing contamination.

Once the primary wick structure is successfully produced, machined to the correct size, and hydrodynamically characterized, the insertion of the wick into the envelope takes place. With a slight interference fit at room temperature between the primary wick and the evaporator body, the envelope must be heated to expand the inner diameter of the envelope. Then the wick is chilled to slightly reduce its diameter and inserted. The design of the wick and the interference fit theoretically results in intimate contact between all the circumferential grooves of the wick and the aluminum envelope. In practice, once the wick is installed the actual contact area is unknown. It is suspected that the physical insertion of the wick shaves and smears the circumferential grooves thereby reducing contact and subsequently the thermal performance of the assembly.

Once the primary wick structure is inserted into the envelope, the KES must be installed. A bi-metallic insertion piece with the knife edge features is evenly pressed into the sintered wick, creating a seal between the inner and outer regions of the primary wick. A bi-metallic interface is necessary because it is desirable to have a KES material with a higher hardness than compared to the Aluminum LHP envelope in order to maintain the integrity of the KES. Experience has shown that a proper seal is not always achieved, and if this KES insertion process fails and

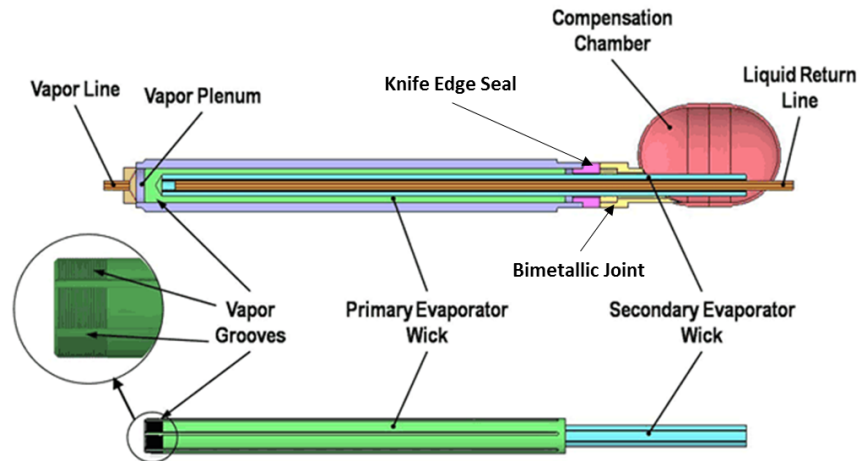


Figure 2. Detailed view of LHP evaporator

reinsertion is attempted, the primary wick is likely to become damaged. This damage typically requires the wick to be scrapped. The envelope may be reused but a new wick must be manufactured. It is also possible for the KES to pass verification testing after assembly but fail later after numerous thermal cycles or vibration testing.

Once the bayonet and secondary wick subassembly are inserted down the bore of the primary wick, the next step in the LHP pump assembly is attaching the front end of the compensation chamber by welding to the bimetals. This process is of concern, due to mismatches in the material coefficient of thermal expansion (CTE) in the Aluminum-Stainless Steel bimetallic transition coupling. Excessive heating of the coupling causes the materials to expand at different rates resulting in a significant stress at the two-material interface. The bimetallic coupling is an off-the-shelf component, and that interface is produced using a friction-stir welding process that has historically been shown to produce an excellent bond between dissimilar metals. However, excessive heating of this component has an inherent high level of risk and has resulted in part failure.

III. Target Application

First the targeted heat load and heat transport distance were determined for a typical CubeSat application. This information is required to determine the maximum pore radius of the 3-D printed primary wicks. A 6U CubeSat was chosen as a basis for design goals based on power levels and popularity. The peak solar power of a 6U CubeSat was determined to be 90W assuming deployable solar panels with 5 faces, each 30cm x 20cm. The radiator area required to reject 90W of heat was calculated to be 0.47m² based on a radiator panel temperature of 253K, sink temperature of 100K, and emissivity of 0.85 as shown in Table 1. This corresponds to about 8 of the 6U faces (20cm x 30cm). The estimated heat transport length to spread heat across this area was calculated to be 3.2m. A conceptual design of what a 6U CubeSat would look like with 5 faces of solar panels and 8 faces of radiators is provided in Figure 3.

Table 1. Radiator area and heat transport length required to reject 90W of heat from a 6U CubeSat

CubeSat Size	6U
Peak Solar Power (W)	90
Evaporator Temp (K)	273
Radiator Panel Temp (K)	253
Sink Temp (K)	100
Emissivity	0.85
Radiator Area (m ²)	0.467
Transport Length (m)	3.2

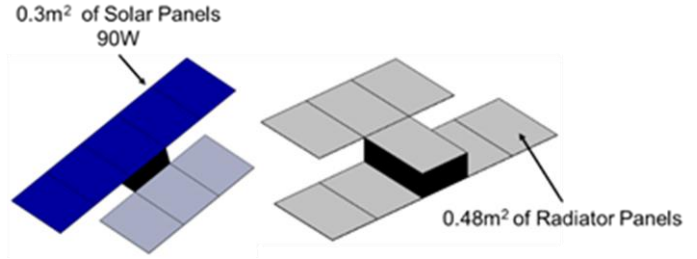


Figure 3. Conceptual design of 6U CubeSat with deployable solar panels and radiators

IV. Pore Radius and Permeability Study

A. Pressure Drop Model

A model was developed to calculate the pressure drop for a 90W LHP with condenser length of 3.2m to determine the required capillary pressure and corresponding pore radius to serve as the goal of the small scale wick parameter study. The total pressure drop in a LHP is the sum of the pressure drop through the vapor grooves, vapor line, liquid line, condenser, and wick and gravity as shown in Eq. 1².

$$\Delta P_{total} = \Delta P_{groove} + \Delta P_{vap} + \Delta P_{liq} + \Delta P_{cond} + \Delta P_{wick} + \Delta P_{grav} \quad (1)$$

For the LHP to operate the capillary pressure in the primary wick must exceed the total pressure drop in the system. The capillary pressure of a porous wick is calculated using Eq. 2

$$\Delta P_{cap} = \frac{2\sigma \cos \theta}{R_p} \quad (2)$$

where σ is the surface tension of the working fluid, θ is the contact angle between the working fluid and wick material (usually assumed to be 0°), and R_p is the pore radius of the wick. Since the capillary pressure is inversely proportional to the pore radius a small pore radius is desired to overcome the total LHP pressure drop. This is why traditionally fabricated LHPs have a primary wick pore radius in the 1-2 μ m range. The pressure drop through the wick was determined using Darcy's Law as shown in Eq. 3

$$Q = \frac{-KA\Delta P}{\mu L} \quad (3)$$

where Q is the volumetric flow rate, K is the permeability of the wick, A is the cross sectional area, μ is the viscosity of the working fluid, and L is the flow length.

Next the pressure drop model was used to study the effect of pore radius on the total pressure drop of the system and capillary pressure available. The results of this study are shown in Figure 4. The pressure drop through the wick decreases with increasing pore radius since permeability is inversely proportional to the pore radius. All other pressure drops remain constant as they are a function of the fluid flow rate and tubing dimensions and independent of wick properties. The available capillary pressure decreases with increasing pore radius. Based on this analysis the pore radius of the 3-D printed wick must be less than 21 μ m for the capillary pressure to exceed the total pressure drop of the system. The margin between available pressure and total pressure drop increases at lower pore sizes. Therefore the goal of the small scale parameter study was to modify the DMLS parameters to minimize the pore radius with a maximum threshold value of 21 μ m.

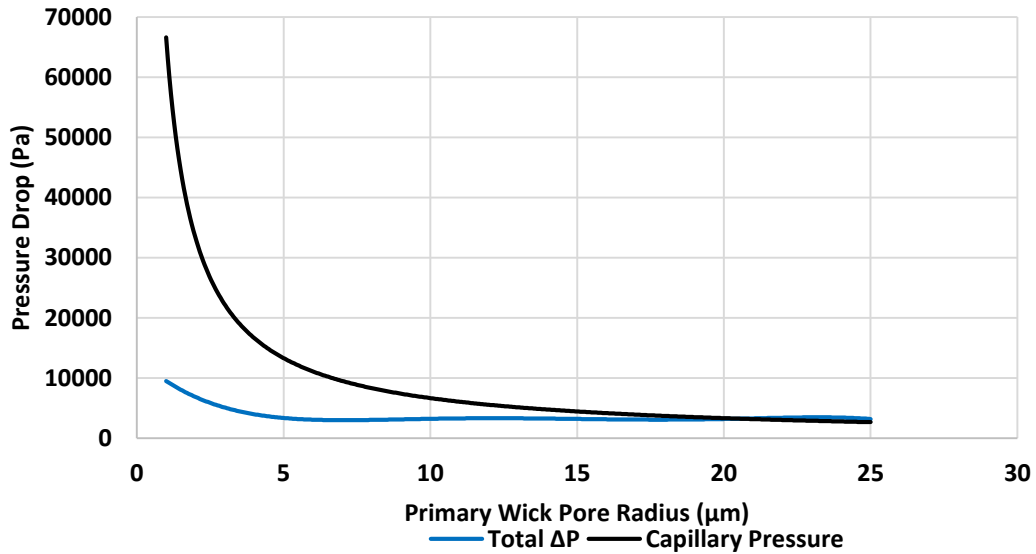


Figure 4. Total pressure drop and available capillary pressure as a function of primary wick pore radius

B. Experimental Testing

A total of 16 cylindrical 3-D printed wick samples were tested. All samples were 1” long and 0.5” in diameter with a 0.08” thick fully dense wall surrounding the porous core as pictured in Figure 5. Two sets of 3 samples were made using PH1 SS (similar to 15-5 SS). Ten samples were made using 316L SS which is the desired material for LHPs.

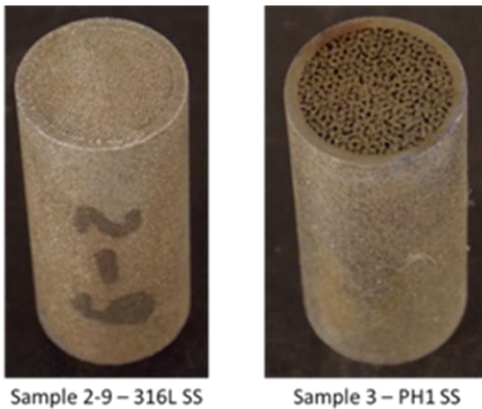


Figure 5. PH1 and 316L SS 3D printed wick samples with fully dense outer wall

First the mass of each sample was measured to determine the porosity of the core. Next the pore radius was measured using a method called the bubble point test. The wick samples were inserted into a rubber tube which is connected to a nitrogen cylinder and placed in methanol. Time was allowed for the methanol to fill the porous core volume through capillary action. Then one side was subjected to pressurized nitrogen. The gas pressure was slowly increased until gas bubbles were able to pass through the wick. The radius of the pores were the calculated using Eq. 4

$$R_p = \frac{2\sigma}{P_b} \quad (4)$$

where R_p is the pore radius, σ is the surface tension of the fluid used (methanol), and P_b is the bubble point pressure. The permeability of each wick sample was measured by pumping methanol through the wick and measuring the pressure drop across the wick and the flow rate of the methanol. The permeability was then calculated using Darcy’s Law as in Eq. 3.

D. Results

The porosity, pore radius and permeability of each sample is shown in Table 2. Flow could not be obtained through samples 2-4 and 2-6 at the maximum pressure of the experimental setup. This indicates that the parts are not porous throughout. Samples 2-8 and 2-13 demonstrated very large pore sizes indicating that large cracks have formed due to incomplete sintering of the metal powder. A plot of permeability vs. pore radius is presented in Figure 6. The relationship between pore radius and permeability of sintered powder wicks is approximated by the empirical Anderson curve shown in Eq. 5

$$K = 0.125R_p^{2.207} \quad (5)$$

where K is the permeability of the wick and R_p is the pore radius. The 316L SS 3-D printed wick samples match up well with the Anderson curve, and achieve smaller pore radii than what was achieved in previous work. This is a significant achievement since the decrease in pore radius from $10\mu\text{m}$ to $6\mu\text{m}$ corresponds to an increase in capillary pumping power from 6.7 kPa to 11 kPa which increases the amount of heat that can be transported by the LHP and the total distance that the heat can be transported.

Based on the results from small scale optimization study the parameters used for samples 2-3 and 2-9 were chosen to be investigated further as part of a repeatability study. Samples 2-10, 2-11, and 2-12 demonstrated favorable permeabilities and pore sizes, but were not chosen due to concerns over loose powder which was present at the surface of the wick. Later this was discovered to be due to a lack of cleaning after the build and not representative of the internal wick. Therefore, in the future these samples will also be investigated further. Six additional samples of 2-3 and 2-9 were fabricated using identical parameters. Porosity, pore radius, and permeability measurements were completed for each sample as described in the previous section. A plot of the results is shown in Figure 6 for visualization. The samples printed using parameters 2-9 formed a tighter grouping with a pore radius ranging from 5.5 to $6.7\mu\text{m}$ while the 2-3 samples ranged from 6.4 to $10.1\mu\text{m}$. Therefore the 2-9 parameters were chosen for fabrication of the primary wick for the LHP prototype.

Table 2. Small Scale Parameter Study Results

Sample	Material	Porosity	Pore Radius	Permeability
		%	um	m ²
1	PH1	32.0	22.7	1.77E-12
2	PH1	31.8	20.0	1.40E-12
3	PH1	31.4	13.7	1.76E-12
4	PH1	34.6	22.7	2.27E-12
5	PH1	35.4	11.4	2.42E-12
6	PH1	35.1	54.9	1.61E-12
2-3	316L	17.2	9.4	2.17E-13
2-4	316L	7.3	9.7	----
2-6	316L	0.0	5.6	----
2-8	316L	34.2	73.2	1.40E-11
2-9	316L	9.3	6.3	3.70E-13
2-10	316L	18.8	6.1	4.30E-13
2-11	316L	14.4	5.8	3.25E-13
2-12	316L	27.3	6.4	7.08E-13
2-13	316L	46.9	94.1	2.84E-10

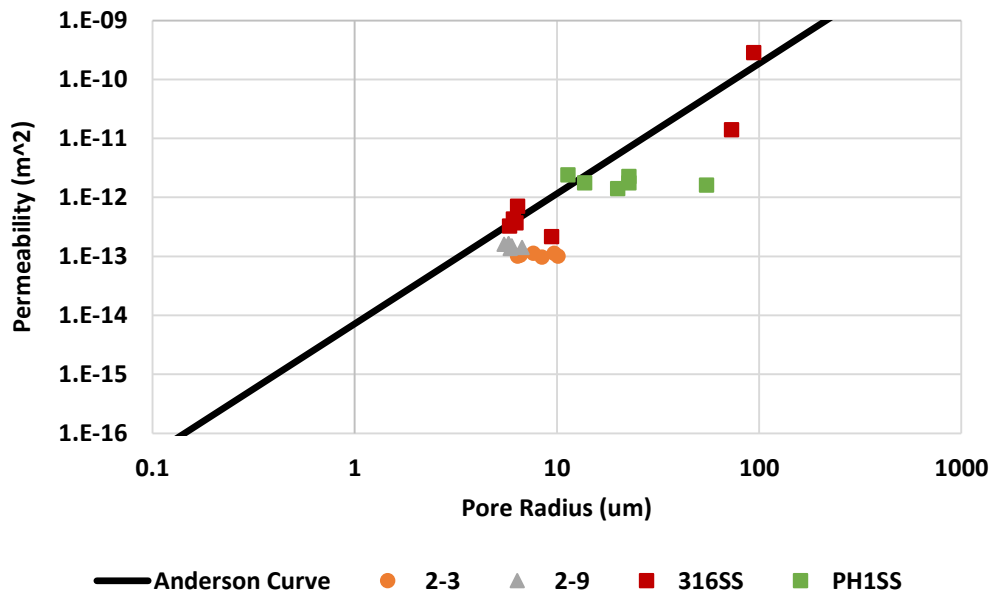


Figure 6. Plot of permeability vs pore radius showing successful reduction in pore radius through optimization of DMLS parameters and repeatability of producing a pore radius $<10\mu\text{m}$ with samples 2-3 and 2-9

V. LHP Prototype

A. Fabrication

The primary wick was designed to be 1" in diameter, which is a standard size, and 4" long to fit inside of a 6U CubeSat. The primary wick must have vapor grooves, a hole for insertion of the secondary wick and liquid return bayonet tube, and a fully dense outside envelope. The fully dense envelope prevents backflow of vapor from the evaporator to the compensation chamber without the use of a knife-edge seal. The primary wick is printed with a thick envelope which is then machined down to create a smooth surface for better contact with the aluminum saddle to reduce thermal resistance. Welding joints have been implemented into the design on both sides for direct welding to the vapor end cap and compensation chamber, eliminating the knife-edge seal and bimetallic joints.

A picture of a 3-D printed primary wick is shown in Figure 7. A total of 4 wicks were printed. The primary wicks were helium leak checked and had a leak rate less than 5×10^{-9} std cc/s, which is ACT's requirement for ammonia LHPs. This is a major accomplishment since the primary wick envelope must be hermetic for long term use on a satellite. The pore radius was measured using the bubble test to be $44 \mu\text{m}$. This is much larger than the $5\text{-}7 \mu\text{m}$ pore radius which was expected. This may be due to the changes in heat dissipation from the location of the laser with a larger part causing incomplete sintering of the metal powder. Due to time limitations a primary wick with a pore radius of $44 \mu\text{m}$ was used for the LHP prototype. In the future the effects that scaling of the 3-D printed design and changing of the geometry have on the pore radius will be investigated to better understand why there was increase in pore radius and prevent this from happening again.

A picture of the completed LHP prototype is shown in Figure 8. The evaporator and condenser sections were joined together with a Swagelok fitting which was welded onto the 1/8 in. condenser line tubing. The condenser tubing length is 3.2m to replicate the length required on a deployable radiator. The entire LHP was helium leak checked and had a leak rate less than 5×10^{-9} std cc/s. The entire LHP assembly was proof pressure tested with methanol up to 600psi which is twice the pressure of ammonia at the maximum operating temperature of 50°C . The methanol was then baked out and the LHP was charged with 35g of ammonia which is enough to completely submerge the secondary wick during startup with gravity.



Figure 7. 3D printed primary wick

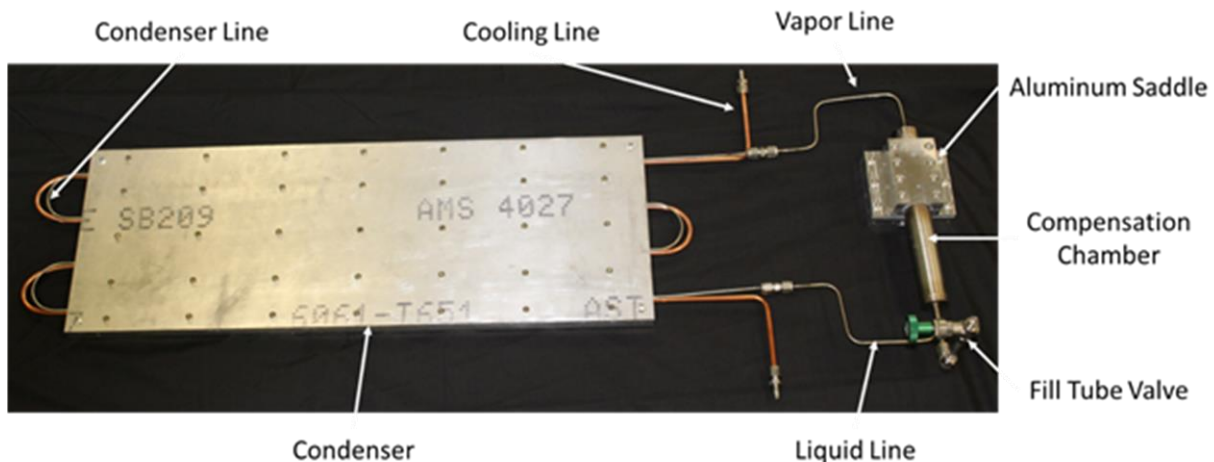


Figure 8. Complete LHP prototype as fabricated

B. Experimental Testing

A schematic of the thermocouple locations for testing the LHP is shown in Figure 9. Insulation was added to minimize heat losses from the evaporator and heat leak into the condenser. A picture of the LHP setup during testing is shown in Figure 10. The chiller pumped coolant at -5°C through the condenser to maintain an average

temperature of about 3°C. For safety, an over temp controller monitored the temperature of the heater block and would shut off power if a temperature of 45°C was exceeded. Additionally two thermostats were wired in series with the cartridge heaters in the heater block which would cut power if a temperature of 50°C was exceeded. The evaporator was raised 13mm (0.5 in.) above the condenser to ensure that the prototype would operate as LHP and not as a thermosyphon.

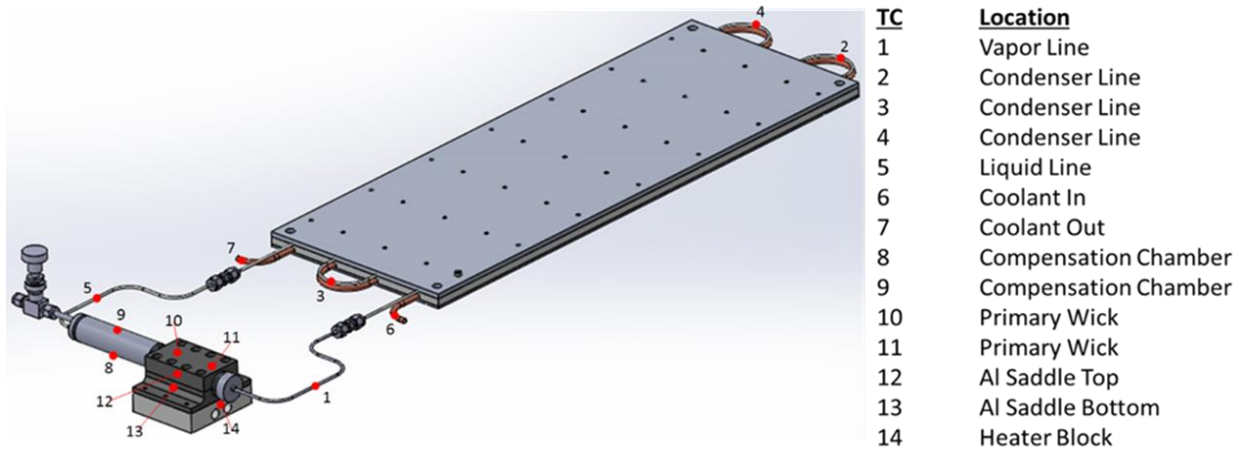


Figure 9. Thermocouple locations used for LHP testing

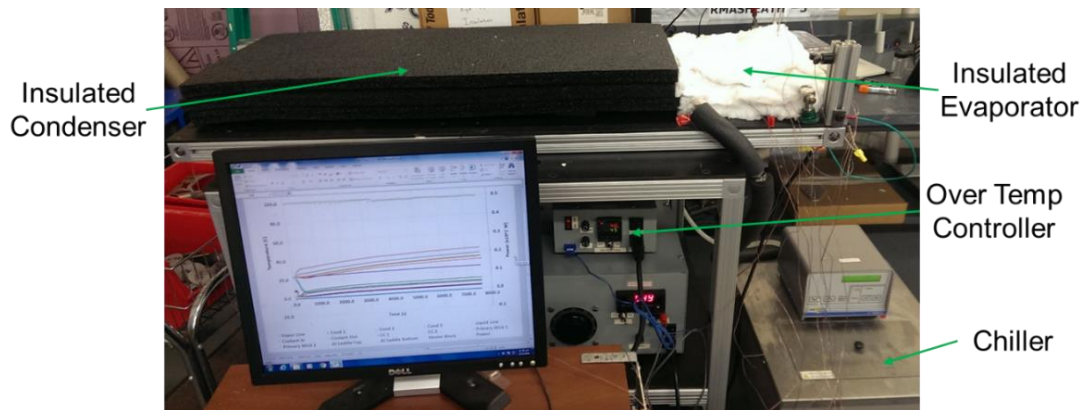


Figure 10. LHP setup during testing

C. Results

Using the pressure drop model described earlier, the maximum power of the LHP prototype was predicted to be 55W. This is less than the original goal of 90W due to the increase in pore size from the small scale samples to the 3-D printed primary wicks. A plot of the prototype testing results with ammonia as the working fluid is presented in Figure 11. A plot of the first 10 minutes is shown in Figure 12 for better visualization of the temperatures during startup. For startup a power of 50W was applied to the heater block. Startup was almost immediate which can be seen by the drop in the liquid line temperature from ambient temperature (22°C) to about 8°C. The drop in liquid line temperature shows that fluid is being pumped through the condenser and subcooled. Also, the coolant outlet temperature rises after startup showing that heat is being transported from the evaporator to the condenser. The temperature of the evaporator continued to increase at a power of 50W and did not level off. Once the evaporator temperature approached the safety shutoff temperature the power was reduced to 45W. At 45W the evaporator temperatures lowered and approached a steady state value. A maximum operating power of 45W is within 20% of the expected value of 55W based on the pressure drop model. The thermal resistance was calculated to be 0.6°C/W based on the temperature difference between the outside of the primary wick envelope and the average coolant temperature in the condenser. This is high for a LHP, but the design was not optimized for thermal resistance due to time constraints. There is room for improvement in the contact resistance between the primary wick and aluminum

saddle, heat leak from the evaporator to compensation chamber, and heat leak from the environment to the condenser and liquid lines.

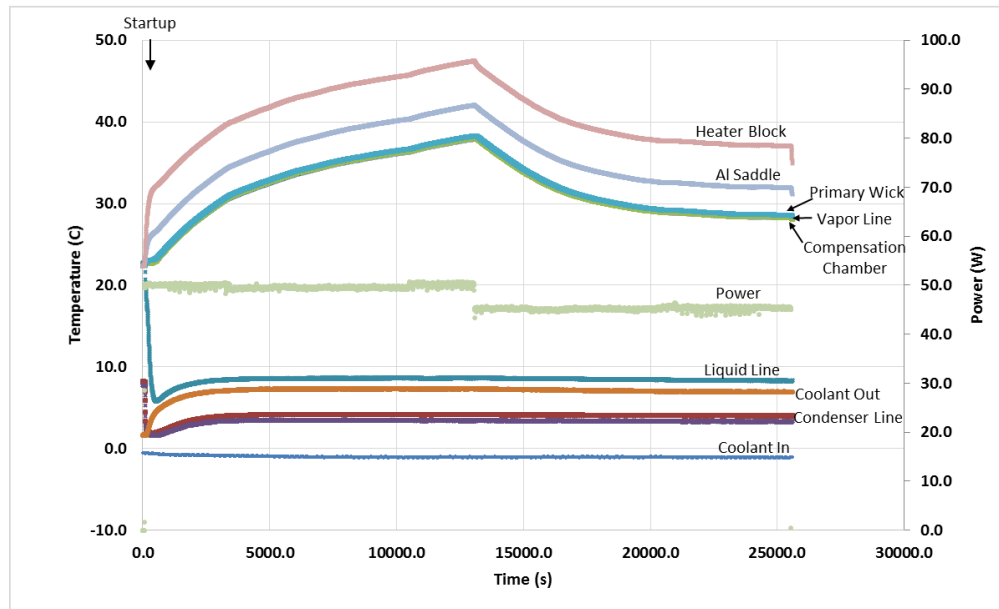


Figure 11. Plot of LHP testing results with ammonia as the working fluid. Steady state was successfully achieved at a power of 45W

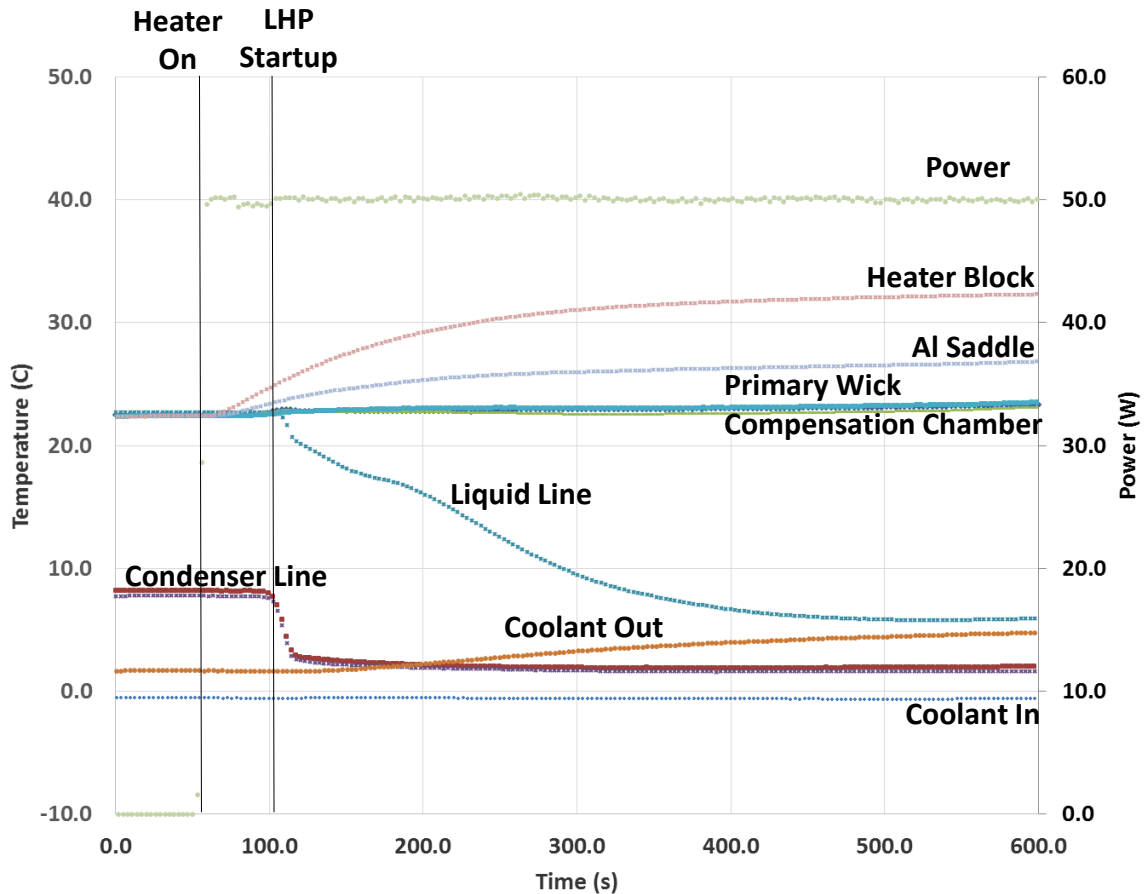


Figure 12. Plot of LHP testing results at startup with 50W heat input

VI. Conclusion

A stainless steel/ammonia LHP with 3-D printed primary wick was successfully designed built and tested. This demonstrates the ability to use a 3-D printed wick with a fully dense hermetic envelope to eliminate the need for a KES. While the power level on the LHP prototype was limited to 45W due to the pore radius of 44 μ m, the results of the small scale pore radius and permeability study indicate that pore radii down to 6 μ m are possible which would increase the maximum power of the LHP to greater than 100W. Additional work is needed to understand the effect of scale up and complex geometries on the pore size so that the necessary adjustments can be made to the DMLS parameters. Once this information is collected 3-D printed primary wicks can be used to significantly reduce the cost associated with LHPs making them a viable option for thermal management of CubeSats, SmallSats, and traditional satellites.

Acknowledgments

This work was funded by NASA through the Small Business Innovation Research (SBIR) program.

References

¹Anderson, W.G., Dussinger, P.M., Garner, S.D., Hartenstine, J.R., and Sarraf, D.B., "Loop Heat Pipe Design, Manufacturing, and Testing – An Industrial Perspective," ASME 2009 Heat Transfer Summer Conference, San Francisco, CA, July 19-23, 2009.

²Ku, Jentung. *Operating characteristics of loop heat pipes*. No. 1999-01-2007. SAE Technical Paper, 1999.